Supplementary Materials for

Dentate gyrus mossy cells control spontaneous convulsive seizures and spatial memory

Anh D. Bui,* Theresa M. Nguyen, Charles Limouse, Hannah K. Kim, Gergely G. Szabo, Sylwia Felong, Mattia Maroso, Ivan Soltesz

*Corresponding author. E-mail: adbui@stanford.edu

Published 16 February 2018, *Science* **359**, 787 (2018)
DOI: 10.1126/science.aan4074

This PDF file includes:

Other Supplementary Material for this manuscript includes the following:
(available at www.sciencemag.org/cgi/content/full/359/6377/787/DC1)

Tables S1 to S4 as Excel files

Materials and Methods

Animals

For mossy cell targeting, both C57BL/6J mice and mice expressing Cre in MCs [Crlr-Cre; C57BL/6N-Tg(Calcrl,cre)4688Nkza/J] (*7*) were used. Mice expressing opsins specifically in DG GCs were generated by crossing mice expressing Cre in GCs [B6.FVB-Tg(Pomc-cre)1Stl/J] with either floxed-STOP HR mice [Ai39; B6;129S-Gt(ROSA)26Sortm39(CAGHOP/EYFP)Hze/J] or floxed-STOP ChR mice (Ai32; Rosa-CAG-LSLChR2H134R-EYFP-deltaNeo). All mice used were more than 6 weeks old and were backcrossed by at least five generations to C57BL/6J. Male and female mice were used. Animals were housed under a 12:12 h light/dark cycle with food and water available ad libitum. For behavioral studies, animals were age matched and underwent the same surgical procedures. All behavioral testing was performed during the light portion of the cycle. All procedures were carried out in accordance with the National Institutes of Health guidelines for animal care and use and were approved by the Administrative Panel on Laboratory Animal Care of Stanford University and by the Institutional Animal Care and Use Committee of the University of California, Irvine.

Stereotactic injection

The mice were deeply anesthetized with isofluorane and placed into a stereotactic apparatus. For ArchT expression, C57BL/6J mice were injected with a virus encoding a Cre-recombinase wheat germ agglutinin (WGA) fusion protein (AAV2-EF1a-mCherry-IRES-WGA-Cre; 1×10^{12} molecules/ml; 2.00 mm posterior, 1.60 mm left, 2.65 mm ventral to bregma), and a virus encoding a Cre-dependent ArchT (AAV5-Flex-ArchT-GFP; 4×10^{12} molecules/ml; 2.00 mm posterior, 1.60 mm right, 2.65 mm ventral to bregma). The virus was delivered via a 2 µl syringe and a 25 gauge metal needle; the injection volume and flow rate were 1 µl at 0.1 µl/min. The needle was left in place after injection for 10 min before slowly being withdrawn. For ChR2 and eNpHR expression, Crlr-Cre mice were injected with the Cre-dependent opsin (for ChR2: AAV5-EF1a-DIO-hChR2(H134R)-EYFP, 4×10^{12} molecules/ml; for eNpHR: AAV5-EF1a-DIO-eNPHR3.0-EYFP, 4×10^{12} molecules/ml; 2.00 mm posterior, 1.60 mm left and/or right, 2.65 mm ventral to bregma). The virus was delivered via a 10 µl syringe and a 33 gauge metal needle; the injection volume and flow rate were 0.2 µl at 0.1 µl/min. The needle was left in place after injection for 10 min before slowly being withdrawn. Non-opsin controls were injected similarly (AAV5-EF1a-DIO-EYFP, 4×10^{12} molecules/ml; AAV5-Flex-GFP, 8×10^{12} molecules/ml). Mice used for behavioral tasks were also implanted with optical fibers (multimode 200 µm diameter, 0.37 NA) either into the dorsal hippocampus (1.70 mm posterior, 1.35 mm left/right, 1.80 mm ventral to bregma) or the ventral hippocampus (3.30 mm posterior, 2.80 mm left/right, 3.70 mm ventral to bregma). Mice used for seizure dynamics studies were implanted as described in "Epilepsy induction and monitoring." Screws and dental cement were used to fix the implant to the skull.

Epilepsy induction and monitoring

The procedures for epilepsy induction and monitoring are similar to those previously described (*10*, *28*). For this model, kainic acid (KA; 40-100 nL, 20 mM in saline) was stereotaxically injected into the left dorsal hippocampus (2.0 mm posterior, 1.25 mm left, and 1.6 mm ventral to bregma) (*8*, *29*) under isoflurane anesthesia at least 3 weeks after virus injection. Non-epileptic control mice were injected with saline only. After two weeks, KA-injected animals developed electrographic and behavioral (Racine stage 4-5), spontaneous, recurrent seizures (*8*). Mice were stereotaxically implanted with bipolar, twisted wire, depth electrodes (1.70 mm posterior, 1.90 mm left, and 1.90 mm ventral with respect to bregma) and optical fibers (3.30 mm posterior, 2.80 mm left and/or right, and 3.70 mm ventral to bregma; 0.37 NA, 200 µm diameter multimode).

The location of the depth electrodes was chosen based on previous studies showing that spontaneous seizures in the KA epilepsy model typically arise from the hippocampal formation ipsilateral to the KA injection site (*8*). For recordings in multiple brain regions (fig. S12), depth electrodes were implanted in the entorhinal cortex (4.90 mm posterior, 3.50 mm left, and 4.00 mm ventral with respect to bregma), hippocampus (1.70 mm posterior, 1.90 mm left, and 1.90 mm ventral with respect to bregma), and primary motor cortex (1.05 mm anterior, 0.90 mm left, and 0.80 mm ventral with respect to bregma). It is important to note, however, that the goal of our study was not to determine the spatial seizure profile or to pinpoint the site of seizure initiation. Data for the GC-HR and GC-ChR2 mice were obtained from recordings performed for a previous study (six animals (*11*)). These animals had optical fibers implanted bilaterally (2.60 mm posterior, 1.75 mm left/right, 1.40 mm ventral with respect to bregma). After recovery from the implant procedure, mice underwent 24 h video and EEG monitoring for closed-loop seizure detection and light delivery.

Closed-loop seizure detection and light delivery

Closed-loop seizure detection and light delivery were carried out as previously described (*10*, *28*). Briefly, the hippocampal EEG signal was analyzed in real-time by a PC running a custom MatLab seizure detection algorithm, and seizures were detected by the software using identifiable spike features. When a seizure was detected, the software randomly decided to deliver light (p=0.5) or no light (p=0.5), resulting in a 50% chance of light delivery for each seizure. Light delivery consisted of a 15 s bout of 10 ms light pulses at 20 Hz for ChR2-expressing mice or 15 s of continuous illumination for ArchT-expressing mice. In both cases, light power was ~3.5-5 mW at the tip of the fiber from a fiber-coupled diode laser of the appropriate wavelength to activate the expressed opsin (473 nm for ChR2, 589 nm for ArchT).

Extraction of electrographic seizure duration, and transition from electrographic to convulsive seizure

The EEG signals surrounding each trigger from the closed-loop system were analyzed offline by individuals trained to analyze EEG signals but blinded to the light condition and type of opsin expression. Post-detection electrographic seizure duration (Fig. 2, figs. S10 and S11) was calculated as total duration of the electrographic seizure minus the detection dwell time (typically 1-3 s) between the beginning of the seizure and the light or sham light delivery. The beginning and end of convulsive seizures were annotated based on the EEG signal and confirmed by analysis of the video recordings. For the convulsive seizures, we focused only on Racine stage 4-5 seizures because the convulsions were more obvious clinically (rearing and falling, loss of postural control), while Racine stage 1-3 seizures were more subjective (mouth, facial, head movements and forelimb clonus) (*13*).

Slice electrophysiology

Whole-cell patch-clamp recordings were done at 33C from 300 μm transverse slices from adult (>6 weeks old) mice using artificial cerebrospinal fluid containing (in mM): 126 NaCl, 2.5 KCl, 26 $NaHCO_3$, 2 $CaCl_2$, 2 $MgCl_2$, 1.25 NaH_2PO_4, and 10 glucose. The patch pipette intracellular solution contained (in mM): 90 K-gluconate, 27.4 KCl, 1.8 NaCl, 1.7 $MgCl_2$, 0.05 EGTA, 10 Hepes, 2 Mg-ATP, 0.4 Na_2-GTP, 10 phosphocreatine, 8 biocytin; pH 7.2; 270–290 mOsm; pipette resistance: 3–5 MOhms. Recordings were done using a Multiclamp 700B, Digidata 1410A, a 3 kHz low pass filter and a sampling rate of 10 kHz. Light was delivered through the epifluorescence port of an Eclipse FN-1, using a Lambda DG-4 with smart shutter and Lambda SC controller and TTL input from a Digidata 1440A.

For the ArchT-expressing MC terminal inactivation experiments (fig. S9), DG GCs were recorded in the whole-cell configuration and voltage-clamped at -75 mV. To isolate excitatory connections, recordings were carried out in the presence of 100 μM picrotoxin and 4 μM CGP 55845 hydrochloride. Series resistance was frequently monitored and 65% compensation was applied. Electrical stimulation of mossy cell axons in the inner molecular layer (IML) to elicit excitatory postsynaptic currents (EPSCs) was performed using an ACSF-filled theta electrode, pulled from a glass theta capillary and broken to a size such that the IML could be stimulated selectively. Stimuli consisted of 5 Hz pulses for a total of 45 s, divided into three 15 s epochs, where light was delivered continuously for 15 s during the second epoch. The recorded traces were analyzed using Clampfit 10.2. The stimulus intensity was set such that the EPSC amplitudes were approximately 50% of the maximum.

Slice electrophysiology data analysis

Resting membrane potential was determined immediately after breaking into the cell. Input resistance was assessed based on responses to intracellularly injected current steps (-150 pA to 500 pA, 1s). Input resistance was defined as the slope of the linear portion of the current-voltage plot generated by traces that did not contain action potential (AP) firing. Time constant was determined as the time to reach 63% of the steady-state response to a minimal current step. AP amplitude was measured from resting potential to peak. Total AP duration was calculated as the width of the spike at baseline. Spike width of the AP at half-amplitude was defined as the width of the spike calculated at half-maximal AP height. Maximal rates of rise and repolarization were calculated from the first derivative (dVm) of the AP waveform. Sag was determined by injecting hyperpolarizing pulses and calculating the ratio of the steady-state response over the peak negative potential. Firing frequency was determined as the maximum number of APs elicited by a 1 s depolarizing current injection (100–600 pA). Fast afterhyperpolarization (AHP) amplitude was defined as the early component that followed the repolarization of an AP and was measured as the difference between the AP voltage threshold and the most negative after-spike potential. Slow AHP was measured as a difference between the AP voltage threshold and the slow component of the decaying membrane potential after the spike (60-120 ms).

Juxtacellular electrophysiology

Juxtacellular recordings were performed in adult Crlr-Cre mice. Anesthesia and surgical procedures were performed as previously described (*30*), with the addition of the implantation of an optical fiber in the right ventral hippocampus (3.30 mm posterior, 2.80 mm right, 3.70 mm ventral to bregma), as described in "Stereotactic injection." Briefly, for mouse head fixation, a stainless steel head bar was affixed to the skull during deep isoflurane anesthesia. On the day of the juxtacellular recording, a small (1 mm) craniotomy was made over the right hippocampus (2 mm posterior, 2 mm right of bregma) under isoflurane anesthesia. The anesthesia was discontinued, and the awake mouse was then placed onto a spherical treadmill, and two glass pipettes containing electrodes were lowered into the brain, one for the local field potential recording (LFP; filled with 1M NaCl) and one for the juxtacellular recording (filled with Ringer solution and Neurobiotin). The LFP was recorded from the CA1 pyramidal layer identified by the maximum power of sharp wave-ripples (SWRs), and the juxtacellular electrode was lowered down in or nearby the hilus where dentate spikes (DSs) could frequently be observed (*30*). Additionally, the LFP electrode was equipped with an optical fiber, so that in addition to examining neuronal activity with illumination into the ventral hippocampus via the previously implanted optical fiber, light could also be delivered into the dorsal CA1 via the LFP pipette. Illumination pattern was the same as for the optogenetic seizure intervention experiments, see "Closed-loop seizure detection and light delivery." Recorded neurons were labeled with the standard juxtacellular labeling method and subsequently were identified visualizing the Neurobiotin content and neurochemical markers

with immunochemistry (*30*), see "Opsin expression validation, immunohistochemistry and histology."

Juxtacellular electrophysiology data analysis

Data were analyzed using custom-written Matlab scripts. To detect spikes from individual cells, juxtacellular recordings were sequentially bandpass filtered (forward and backward 4th order Butterworth filter, 0.3-10 kHz), filtered using the non-linear energy operator and smoothed using a 0.5 ms averaging window. Local maxima in the resulting signal that exceeded a defined threshold (3 times the median absolute deviation of the signal) were labeled as spikes. For each spike, the AP waveform was extracted from the bandpass-filtered signal using 3 ms cropping window centered on the spike maximum and normalized to its maximum. When more than one cell was present in the recording, spikes were sorted using *k*-means clustering applied to the waveform. To avoid false detections, spikes with a waveform that was significantly different than the median waveform of the cluster (root mean squared distance of the waveform to the median larger than 3 times the median absolute deviation) were discarded.

Object location memory and object recognition memory paradigms

Prior to training, mice were handled 2 min/day for 5 days, then habituated in the experimental apparatus 5 min/day for 6 days in the absence of objects, as described in (*15*, *31*). Briefly, during training, the mice were placed in the presence of two identical objects (e.g. 100 ml beakers) for 10 min and allowed to freely explore. During testing (24 hours after training), the mice were placed again in the presence of two objects. For OLM, the objects were the same, but one object was in the same location as during training, while the other object was moved to a novel location. The distance moved for the moved object was 11 cm. For ORM, one object was replaced with a novel object, but the location remained the same as during training. The determination of which object was moved or replaced was randomized and balanced. Light stimulation was delivered continuously either during the training or testing phase (bilaterally into the hippocampus, 589 nm, 5-7 mW at the tip of each fiber). Training and testing trials were video-recorded and analyzed by a researcher blind to the injection scheme, using software from (*31*). Object exploration was quantified as the amount of time the mouse's nose spent touching the object or was $<$1 cm away from the object. The relative exploration times were expressed as a discrimination index (D.I. = $(t_{novel} - t_{familiar}) / (t_{novel} + t_{familiar}) \times 100\%$). Mice that explored the objects for less than 3 s total during either training or testing were removed from further analysis. Mice that exhibited an object preference during training (D.I. $>$ 20) were also excluded. These criteria were pre-established (*15*). Raw data for object exploration during OLM and ORM tasks are shown in Table S4.

Elevated plus maze

The elevated plus maze consisted of two open arms (30 x 5 cm) and two enclosed arms (30 x 5 x 20 cm) which extended from a central platform (5 x 5 cm) to form a plus. The apparatus was elevated to 30 cm above the floor. Mice were placed individually in the center of the maze facing the open arm opposite to the experimenter. The percentage of time spent in the open arms was scored using AnyMaze, and movement was tracked relative to the center of the mouse body. Between subjects, the maze was cleaned with 70% ethanol. Testing with epileptic/non-epileptic mice was 5 min total. Testing with eNpHR-/eYFP-expressing mice was 15 min total and was divided into three 5 min epochs. The mice received no light during the first epoch, light stimulation during the second epoch, and no light during the third epoch. During the light on epoch, mice received 5 min of continuous illumination bilaterally into the hippocampus (589 nm, 5-7 mW at the tip of the fiber).

Opsin expression validation, immunohistochemistry and histology

To determine specificity of opsin expression in MCs, animals were deeply anesthetized and perfused transcardially with 4% paraformaldehyde. 60 μm coronal brain sections were stained for GluR2/3 (rabbit anti-GluR2/3, 1:200) or for GABA (rabbit anti-GABA, 1:250). Selectivity of opsin expression was quantified by comparing GFP or eYFP cells with GluR2/3-positive cells or GABA-positive cells, and the degree of MC loss was quantified by examining GluR2/3 immunoreactivity and using the 49,6-diamidino-2-phenylindole (DAPI) stain to identify cells. Measurements were done using a confocal microscope and the optical dissector method, using every slice for the ArchT-expressing mice in Fig. 1H, top and every fourth section throughout the entire anterior–posterior extent of the hippocampus for all other measurements. For the juxtacellular recordings, Cell 3v/d was identified as CB1+ with staining for CB1 (guinea pig anti-cannabinoid receptor type 1, 1:1000), Cell 5v/d was identified as an IN based on morphology, and Cell 6v was identified as an axo-axonic cell (AAC) based on the morphology, specifically the unequivocal presence of the characteristic candelabra-like rows of boutons, as well as with staining for parvalbumin (rabbit anti-parvalbumin, 1:2500).

Statistical analysis

Electrographic seizure durations:
Differences in the distribution of post-trigger seizure duration between the light and sham triggers (Fig. 2, figs. S10 and S11, Table S3) were analyzed at the group level (animals pooled by type of opsin) using the two-tailed Mann-Whitney *U* test. This tests the null hypothesis that a randomly selected seizure from the light group is equally likely to be shorter as it is to be longer than a randomly selected seizure in the no light group, which we phrased in the text as "light has no effect on seizure duration." Outcomes of light vs. no light conditions on post-detection seizure durations were also compared within each individual animal using the Mann-Whitney test. Data in figures 2 and 3 and supplementary figures 10 and 11 report the median seizure duration, along with the 95% CI computed by bootstrap (n = 10,000 bootstraps). For each animal, a random set of ~130-600 electrographic seizures was included in the analysis (Table S3). This number allows us to detect a 3 s change in seizure duration with a 20% false negative rate (power estimated for a two-tailed t-test at 0.05 level with a standard deviation in seizure duration of ~13 s).

Convulsive seizure durations:
Group level and animal level statistical analysis of the convulsive seizure duration was done in a similar manner as for the electrographic seizure analyses.

Occurrence of convulsive seizures:
To compare the number of convulsive seizures occurring following either light or no light delivery in epileptic MC-ChR2, MC-ArchT, MC-GFP animals (Fig. 3), we used a binomial test with a success probability of p=0.5. This tests the null hypothesis that behavioral seizures are equally likely to occur following light or no light delivery, which would be expected if light had no effect on seizure progression since each trigger independently delivered light with a 50% probability. The binomial test was also used for group data (animals pooled by type of opsin, Fig. 3D), and the test results were presented as the measured fraction of behavioral seizures occurring following light delivery, side-by-side with the expected fraction and its 95% CI under the null hypothesis (binomial distribution, p=0.5). Occurrence of convulsive seizures in opsin-expressing GC animals was analyzed in a similar manner (fig. S11). Only appropriately timed triggers for behavioral seizures (i.e., triggers during the electrographic only portion of the seizure, before the emergence of overt convulsions) were included in the analysis. Effect of post-seizure triggers (fig. S14) was quantified similarly, except that the triggers used were the first triggers occurring after the end of each convulsive seizure. Starting from the beginning of the closed-loop intervention, each animal was monitored during its entire lifespan or until the EEG signal became cor-

rupted (e.g., due to excessive motion during seizures), amounting to up to 6 months of continuous recording per animal. For each group, at least 2-3 animals were recorded to obtain $>$37 seizures total, which gives a 0.2 false negative rate for the binomial test (power $\beta = 0.8$) to detect a 20% change in seizure frequency between light and no light at the 0.05 level. Non-significance at the 0.8 power level was reported as n.s. in the text.
To verify that the effect of light stimulation on convulsive seizure occurrence is not a function of circadian rhythm, we repeated the analysis separately on convulsive seizures that occurred during the daytime (7am-7pm) and on those that occurred during the nighttime (7pm-7am).

OLM, ORM, EPM tests:
Data from OLM, ORM, and EPM were analyzed using the unpaired Welch's t-test to compare the performance of non-epileptic vs. epileptic, or eYFP vs. eNpHR mice. This test does not require equal variance between groups but assumes normality, which was verified using the Kolmogorov-Smirnov test (*P $<$0.05).
Statistical analysis was conducted using Matlab.

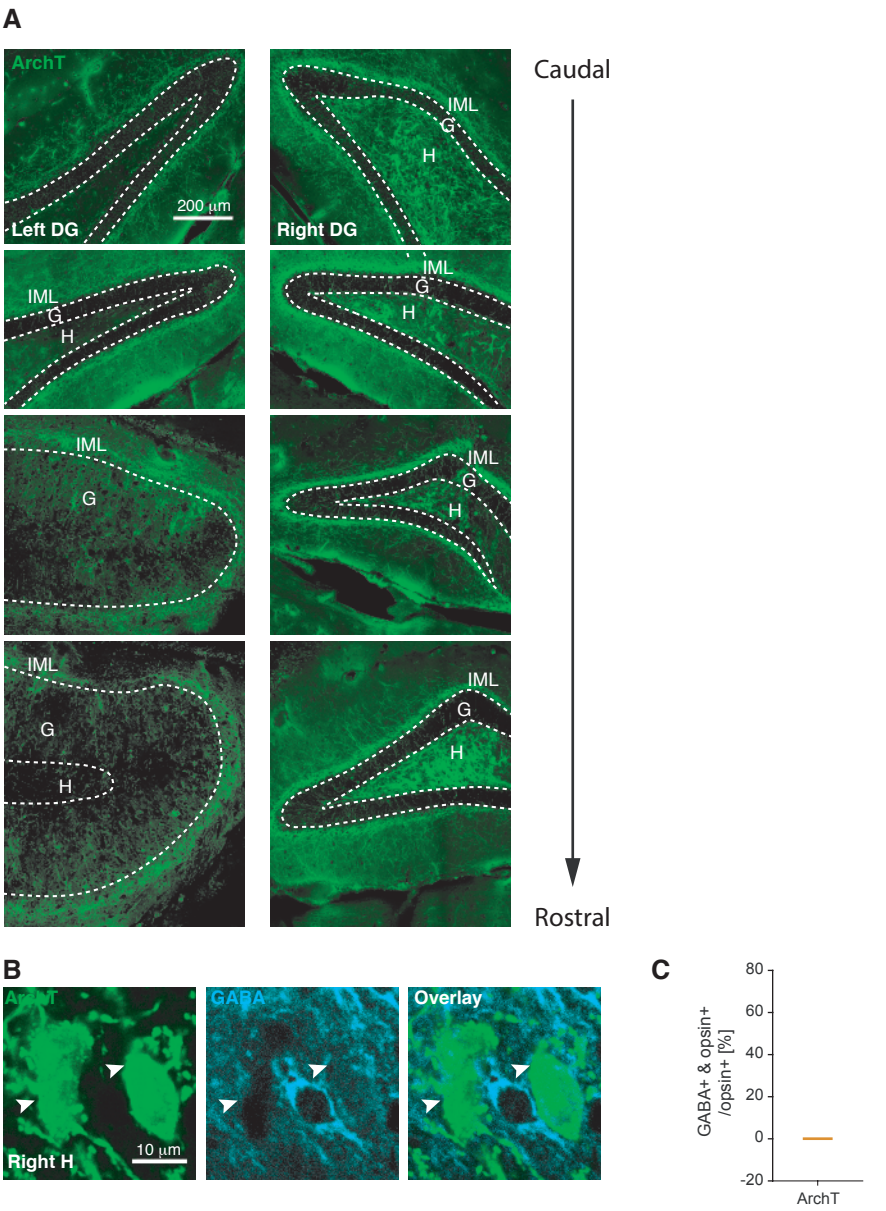

Figure S1. Specificity and extent of ArchT transduction in MCs. (A) Confocal images of ArchT expression (green) in MC showing the extent of transduction caudally to rostrally along the hippocampal longitudinal axis. Left: ArchT expression in MC axon terminals in the left DG. Right: ArchT expression in hilar MCs in the right DG. **(B)** High magnification images of the right hilus. ArchT-expressing MCs are identified via GFP expression (arrowheads) and do not show colocalization with GABA. **(C)** Opsin expression specificity, quantified by the proportion of ArchT+ neurons that were also GABA+ (n = 3 mice). ArchT+ neurons were labeled using the WGA-Cre system. G, granule cell layer; H, hilus; IML, inner molecular layer.

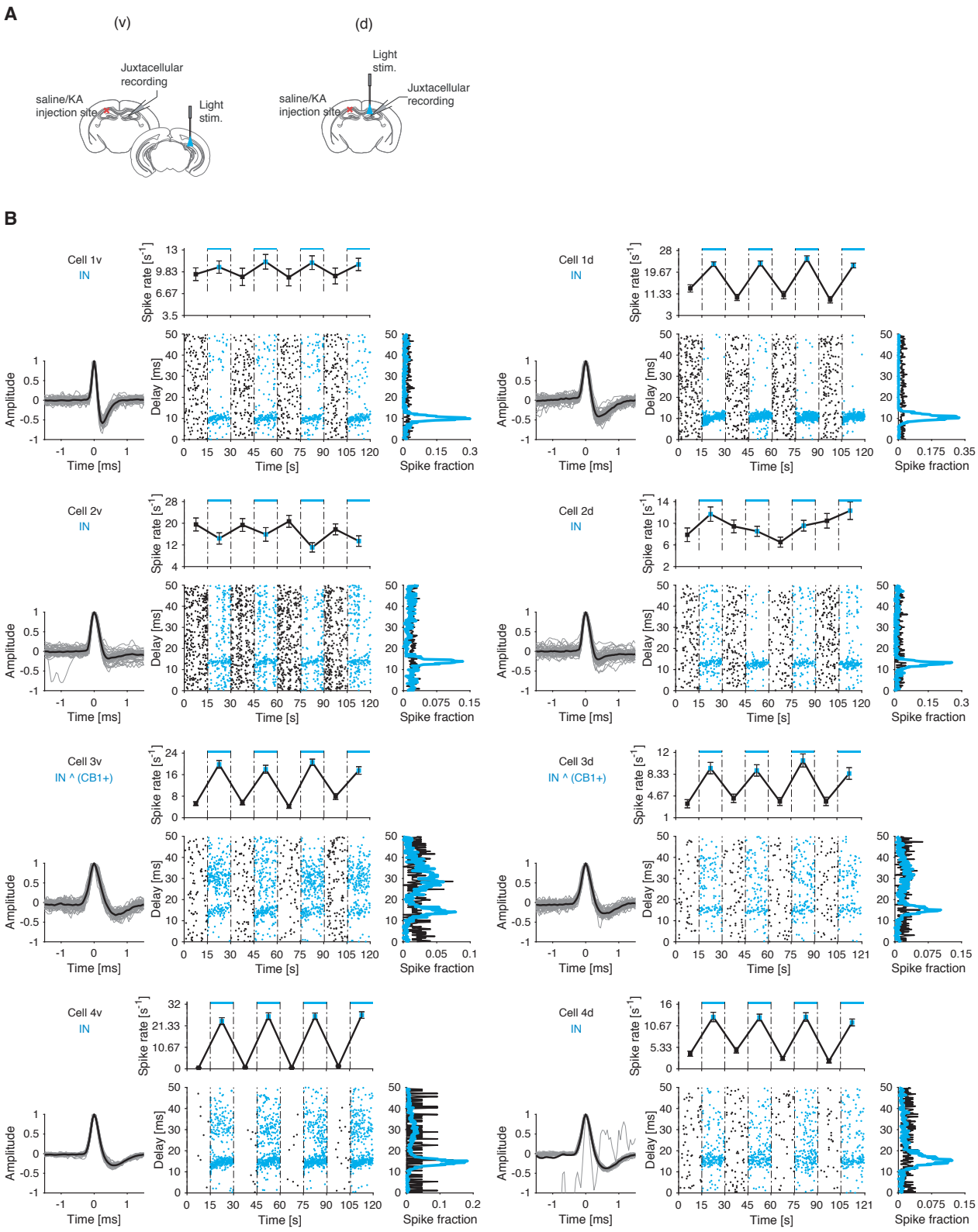
A
(v)
Juxtacellular recording
saline/KA injection site
Light stim.
(d)
Light stim.
saline/KA injection site
Juxtacellular recording
B
Cell 1v
IN
Cell 1d
IN
Cell 2v
IN
Cell 2d
IN
Cell 3v
IN ^ (CB1+)
Cell 3d
IN ^ (CB1+)
Cell 4v
IN
Cell 4d
IN
Spike rate [s-1]
Amplitude
Time [ms]
Delay [ms]
Time [s]
Spike fraction

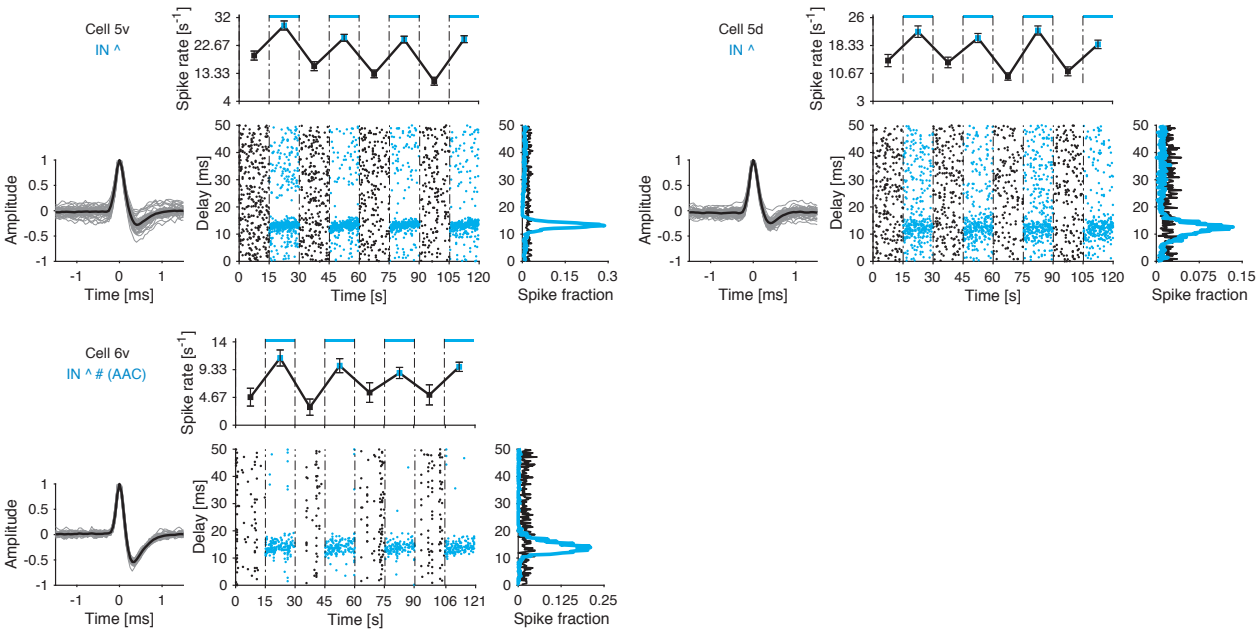

Figure S2. Selective MC optogenetic stimulation modulates the activity of juxtacellularly recorded dentate gyrus interneurons in non-epileptic and epileptic mice. (A) Schematic of the placement of the juxtacellular recording electrode and the optical fibers used for ventral (v) and dorsal (d) light delivery. **(B)** Firing properties of individual cells. For each recorded unit, data are shown as follow. Left: amplitude-normalized waveform of 30 randomly selected spikes (thin, gray lines) and average unit waveform (thick, black line). Center, top: MC photostimulation (20 Hz train of 10 ms pulses for 15 s, blue bar) modulates interneuronal cell firing rate. Data are shown as mean firing rate ± s.e.m, over the course of 4 light on/light off cycles. Most recorded interneurons exhibit increased firing upon MC stimulation, except for Cell #2, which shows reduced firing during the light on epochs. Center, bottom: Phasing of the neuron activity with the laser pulse train. Scatter plot shows for each spike the delay between the onset of the laser pulse (light on epochs, blue data) or sham pulse (light off epochs, black data) and the spike. Right: Distribution of the laser-to-spike delay (blue) and the sham-to-spike delay (black). These were obtained using all the unit spikes recorded during the light on and light off epochs, respectively. d, dorsal light delivery; v, ventral light delivery; ^ confirmed cell identity; # epileptic mouse; CB1+, cannabinoid receptor type 1 interneuron; AAC, axo-axonic cell. For statistical information about each unit recording (e.g., animal of origin, firing rates, spike properties), see Table S2. Cell 6v replotted from Fig. 1H.

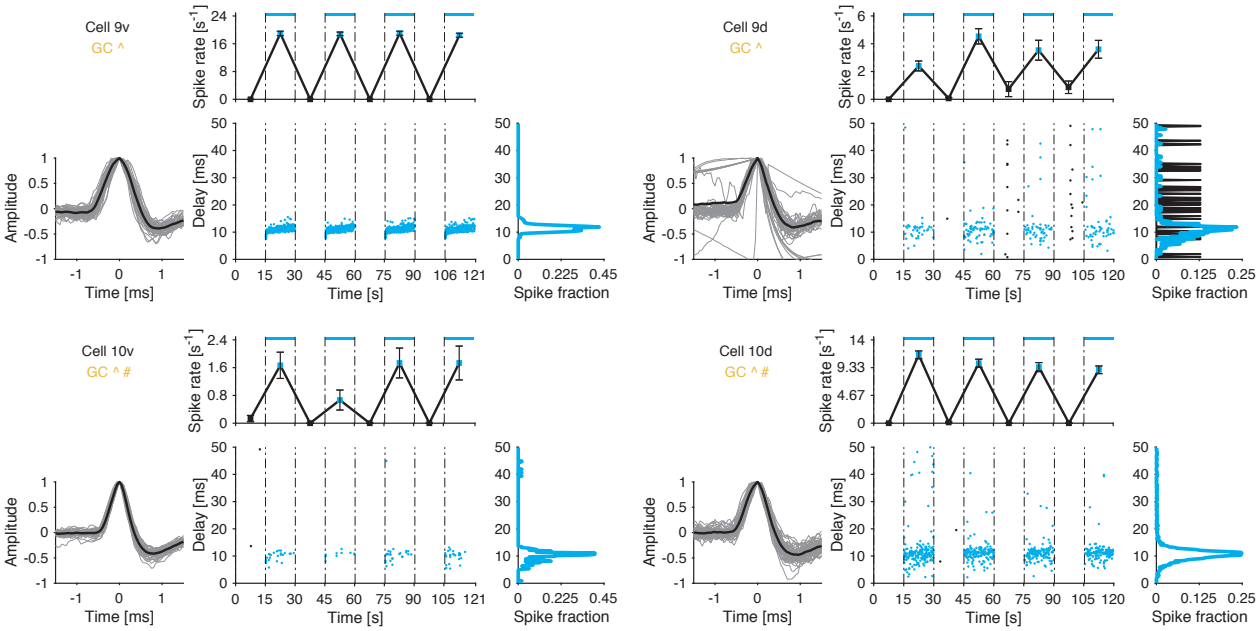

Figure S3. Selective MC optogenetic stimulation increases the activity of juxtacellularly recorded GC in non-epileptic and epileptic mice. Data are shown as in fig. S2B. Cell 10v re-plotted from Fig. 1I.

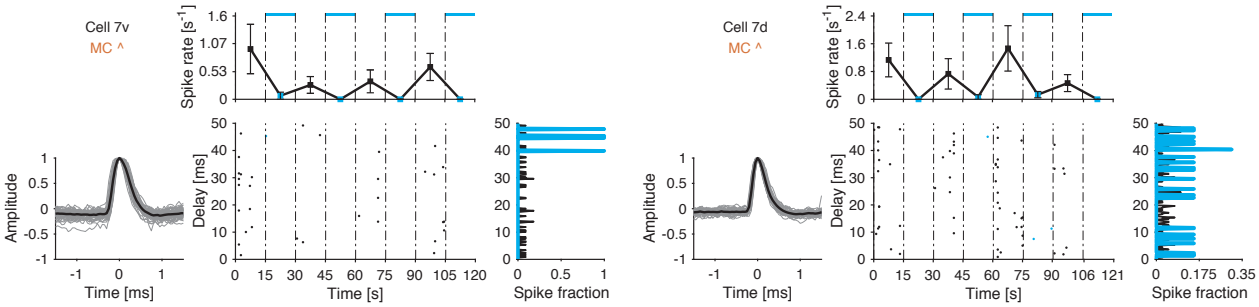

Figure S4. Selective MC optogenetic stimulation inhibits the activity of juxtacellularly recorded opsin-negative MC in a non-epileptic mouse. Data are shown as in fig. S2B.

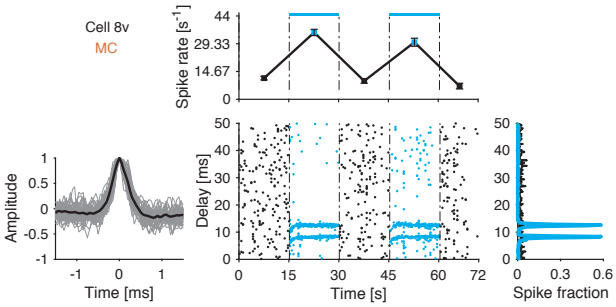

Figure S5. Optogenetic response of a putative ChR2-positive MC recorded juxtacellularly in a non-epileptic mouse. Data are shown as in fig. S2B.

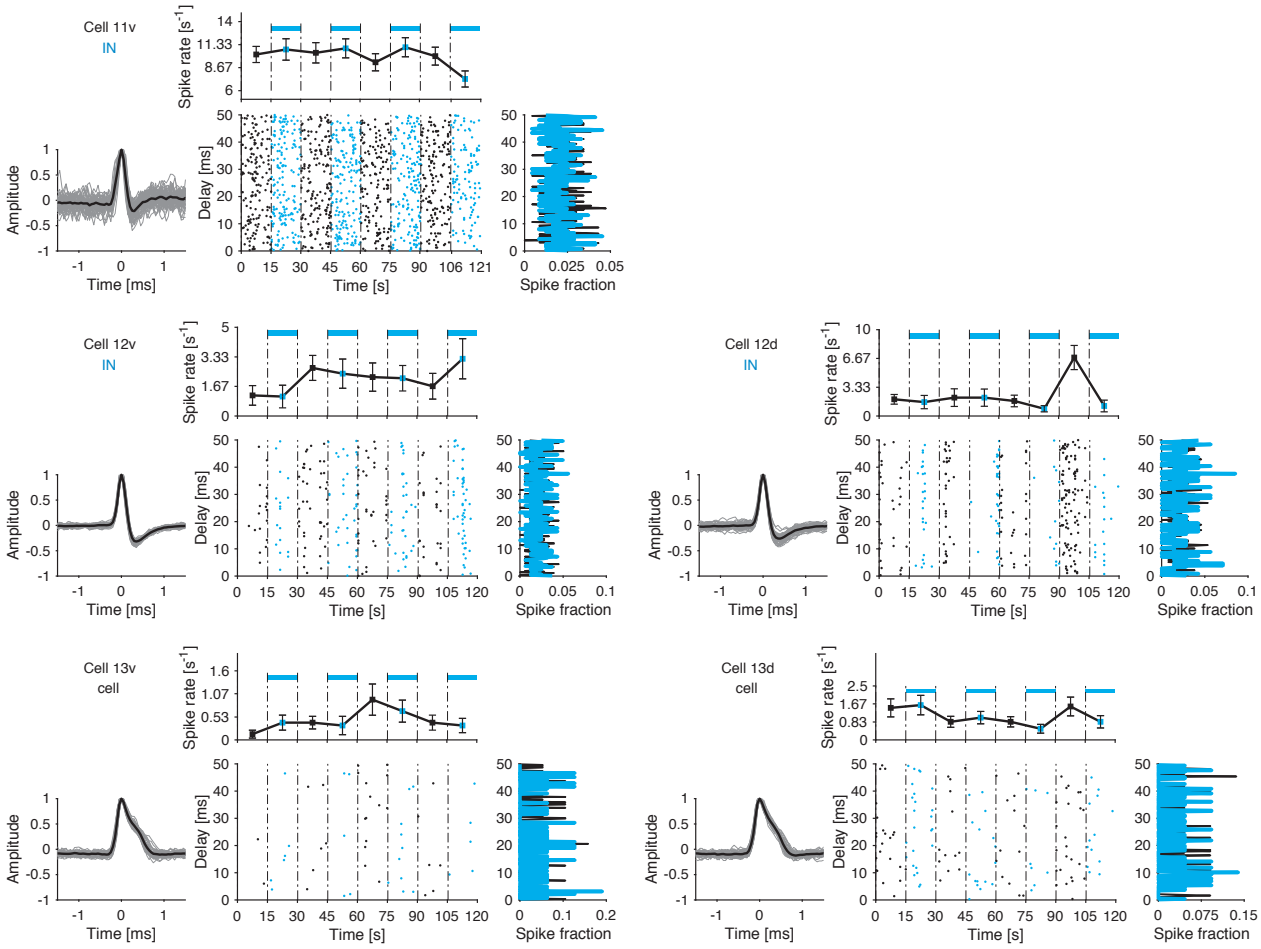

Figure S6. Light delivery to non-opsin-expressing control mice does not modulate the activity of juxtacellularly recorded dentate gyrus interneurons in non-epileptic mice. Data are shown as in fig. S2B.

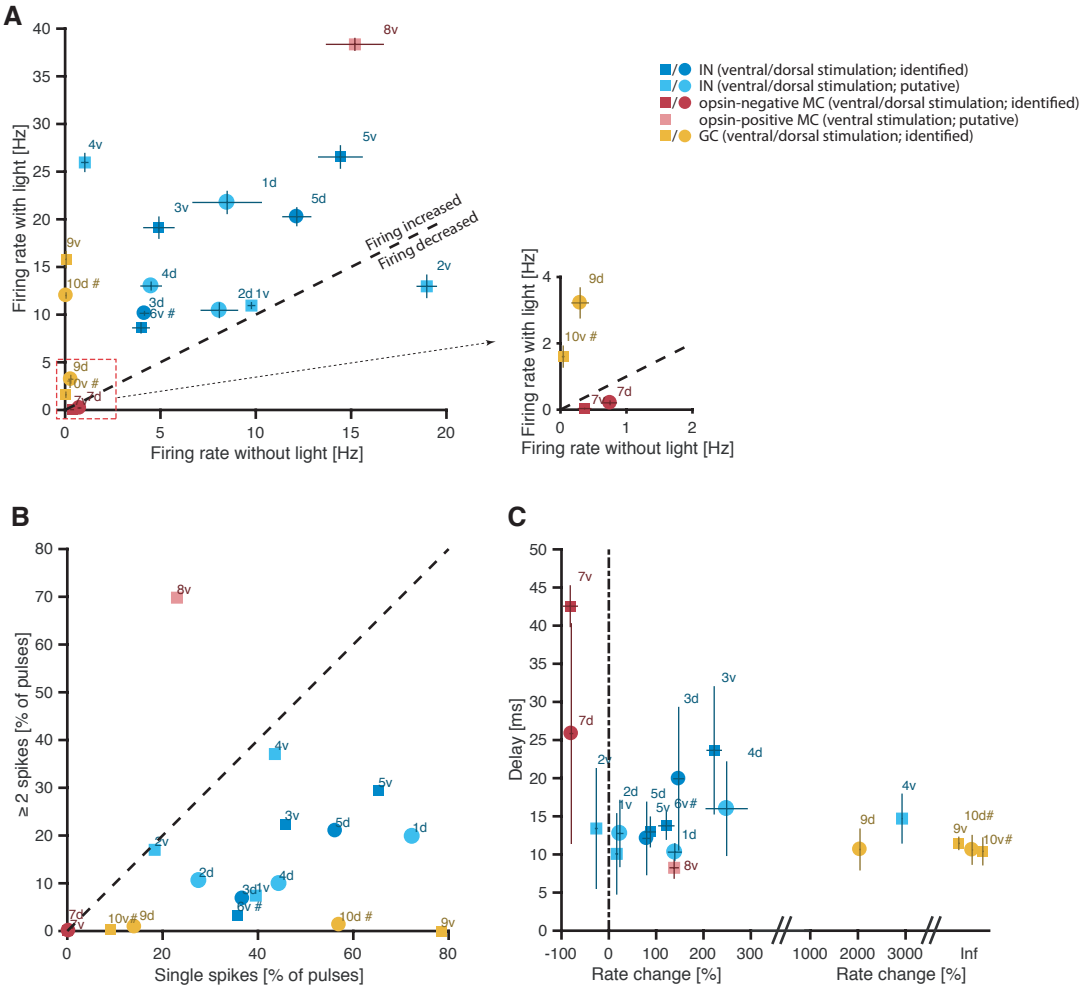

Figure S7. Summary of effect of optogenetic MC excitation on individual juxtacellularly-recorded dentate gyrus neurons in non-epileptic and epileptic, ChR2-expressing mice. (**A**) Juxtacellular measurement of the firing rate of individual dentate cells with and without stimulation of MC with light. Data are shown as the average rate ± s.e.m. of INs (n = 6 cells), opsin-negative MCs (n = 1 cell), GCs (n = 2 cells), and a putative opsin-positive MC (n = 1 cell). Stimulation is either ventral (squares) or dorsal (circles). **(B)** Firing properties of the dentate cells shown in **(A)** during light on epochs. Data are shown as the fraction of laser pulses which result in either single spikes or 2 spikes. **(C)** Scatter plot of the median delay between the onset of the laser pulse and the action potential as a function of the rate change (rate during light on/rate during light off×100%) of the dentate neurons shown in **(A)**. # Data are from epileptic animals, all other data are from non-epileptic animals.

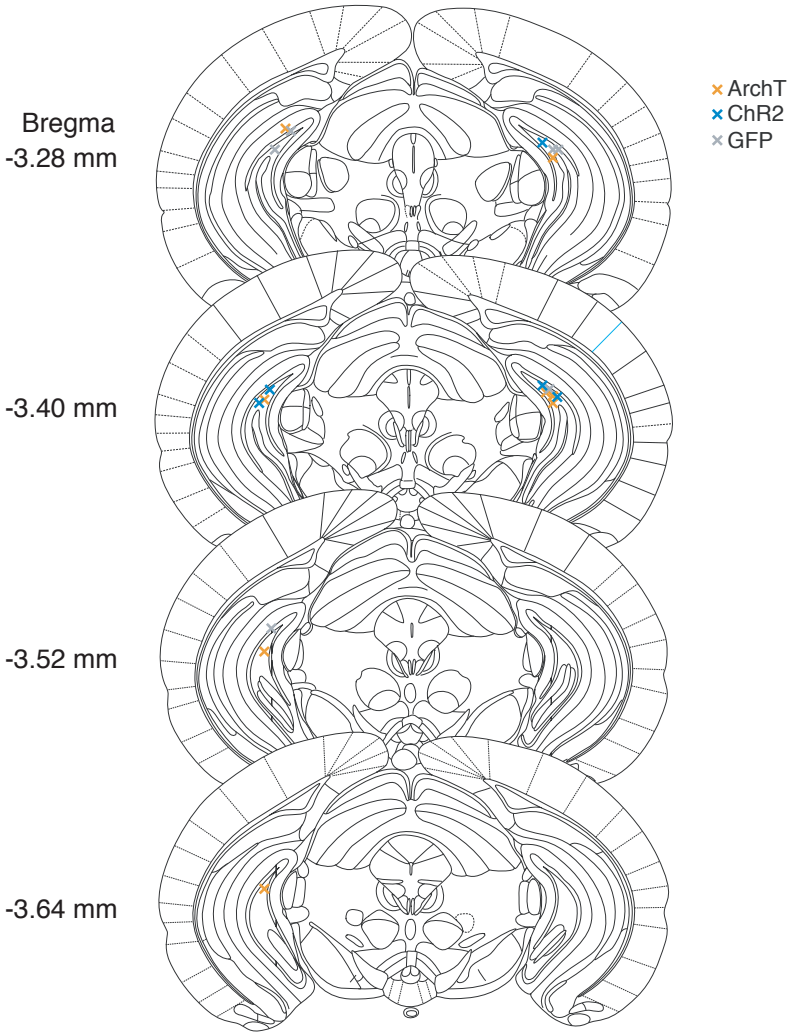

Figure S8. Post-hoc verification of optical fiber locations for chronically epileptic mice with optogenetic seizure intervention. (n = 4 ArchT, n = 5 ChR2, n = 3 GFP).

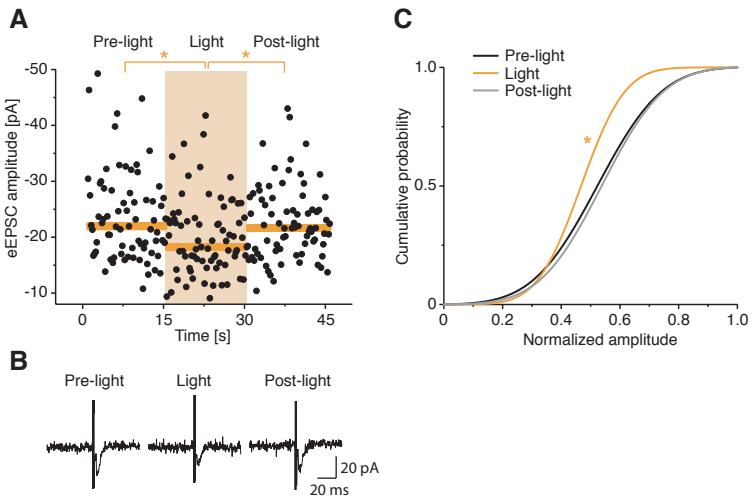

Figure S9. Illumination of ArchT-expressing MC axon terminals is sufficient to reduce electrically-evoked neurotransmitter release. (A) Selective illumination of ArchT-expressing MC axon terminals reduces the amplitude of evoked excitatory postsynaptic currents (eEPSC; mean amplitude, orange bar) in a postsynaptic GC in an acute slice from an epileptic mouse. Light (590 nm; orange box) was delivered only during the second of three 15 s epochs. **(B)** Traces of GC eEPSCs before (left), during (middle), and after (right) light delivery. **(C)** Cumulative distribution of postsynaptic GC eEPSC amplitudes before, during, and after illumination (n = 5 GCs; $*P < 0.05$, two-tailed Mann-Whitney test).

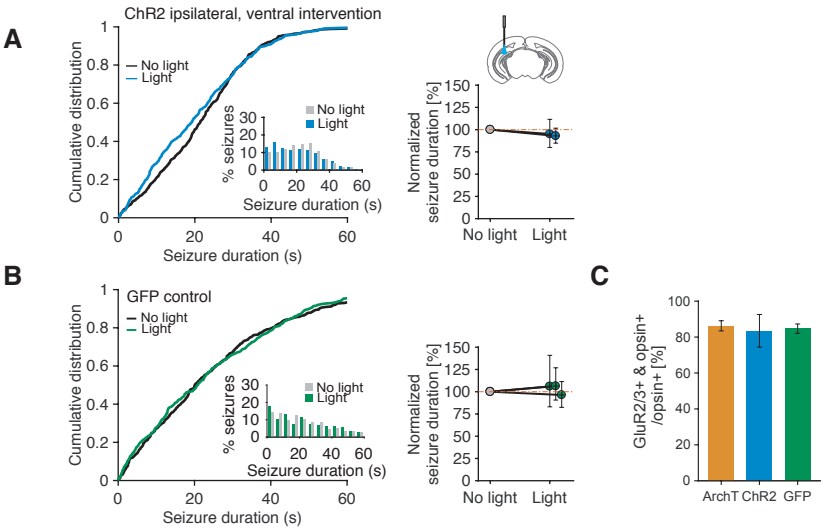

Figure S10. Optogenetic stimulation of MCs ipsilateral to the kainate injection site and light delivery in opsin-negative control mice do not affect electrographic seizure duration. Effect of **(A)** light delivery to the ventral hippocampus in mice expressing ChR2 ipsilateral to the kainate injection site and **(B)** illumination in non-opsin-expressing mice. Left: cumulative distribution and probability density (inset) of the seizure duration following start of light or no light delivery (all animals combined, N = 714|733 seizures, n = 2|3 animals, for ChR2-|GFP-expressing mice; $P > 0.05$ Mann-Whitney U test). Right: seizure duration. Data are shown as the normalized difference in seizure duration between the light and no light events and 95% CI for each individual animal as in Fig. 2. ($P > 0.05$ for each animal, two-tailed Mann-Whitney U test). **(C)** Opsin expression specificity, quantified by the proportion of ArchT+, ChR2+ and GFP+ neurons that were also GluR2/3+ (ArchT and ChR2 replotted from Fig. 1; N = 38 slices, n = 3 mice for GFP+).

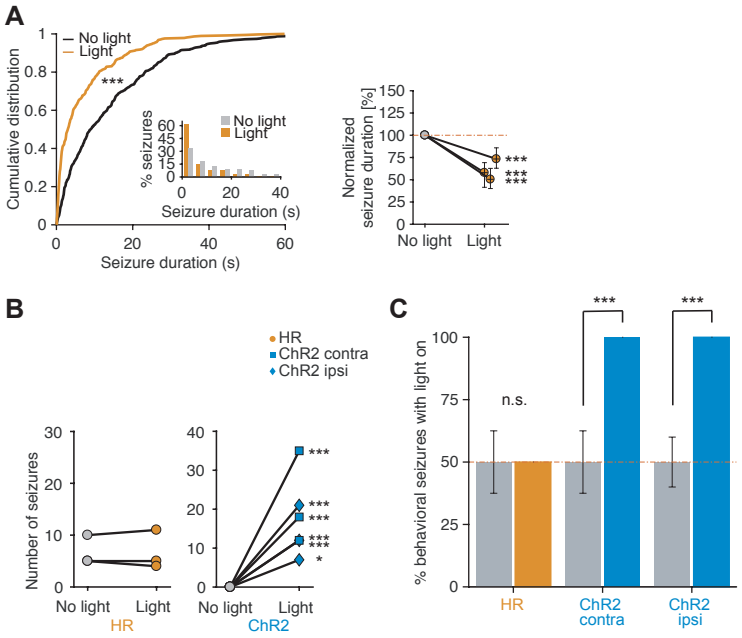

Figure S11. Dentate gyrus (DG) granule cell (GC) optogenetic perturbation during spontaneous seizures in chronic TLE. (A) On-demand inhibition of DG GCs significantly shortens spontaneous electrographic seizures. Left: cumulative distribution and probability density (inset) of the seizure duration following start of light or no light delivery (all animals combined, N = 841 seizures, n = 3 animals; $***P < 0.001$ Kolmogorov-Smirnov). Right: seizure duration. Data are shown as normalized difference in seizure duration between the light and no light events and 95% CI for each individual animal ($***P < 0.001$, Mann-Whitney U test). **(B)** Left: for each measured animal (n = 3), photoinhibition of DG GCs does not affect the occurrence of behavioral seizures. Right: DG GC photostimulation significantly increases the occurrence of behavioral seizures (n = 6). $*P < 0.05$, $***P < 0.001$, two-tailed binomial test. **(C)** On-demand inhibition of HR-expressing GCs has no effect on the occurrence of behavioral seizures, and photostimulation of ChR2-expressing GCs induces behavioral seizures. Solid colored bars represent the fraction of convulsive seizures occurring after light delivery. White bars represent the expected fraction 95% CI of seizure occurring with light, under the null hypothesis that light delivery has no effect. $***P < 0.001$, two-tailed binomial test. Data from **(A)** and ChR2 data from **(B & C)** are re-analyzed from data presented in Krook-Magnuson et al. 2015. HR data in **(B & C)** are new data from this study.

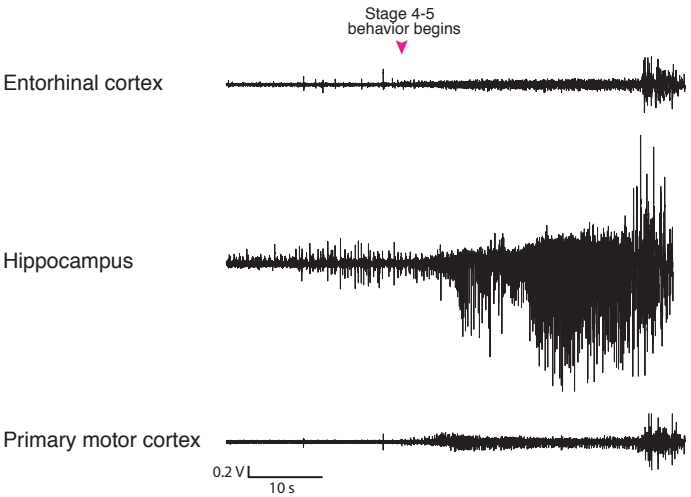

Figure S12. Electrographic-to-behavioral seizure recorded simultaneously in the entorhinal cortex, hippocampus, and primary motor cortex.

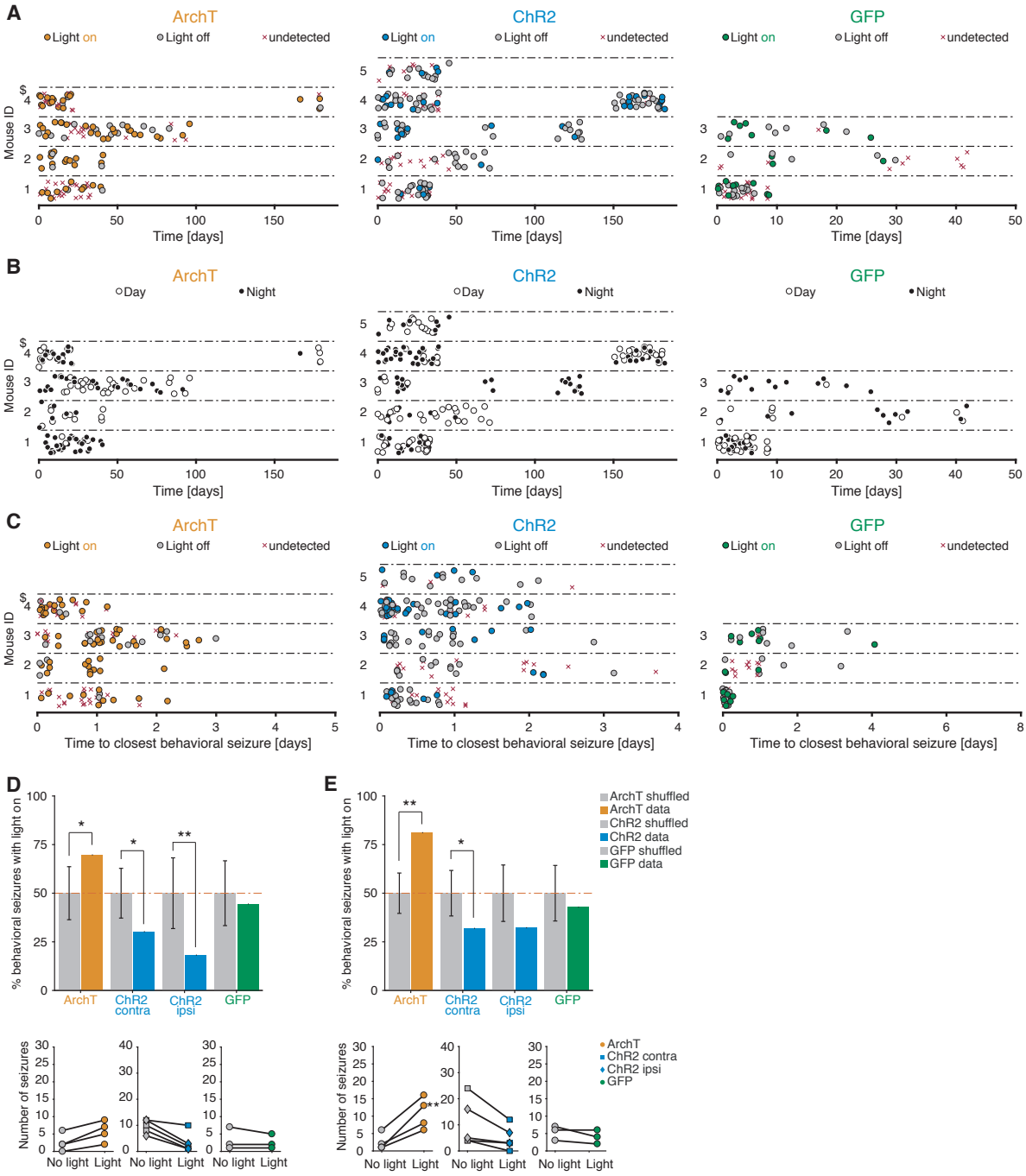

Figure S13. Effect of optogenetic modulation of MCs on convulsive seizures occurrence is similar during day and night periods. (A) Timeline of behavioral seizure occurrence for each recorded animal (ArchT-|ChR2-|GFP-expressing mice at left|center|right) and light treatment during the electrographic phase of the seizure.

(B) Timeline of the behavioral seizures occurring during the daytime and nighttime for each recorded animal. **(C)** Scatter plot showing the dwell time between successive convulsive seizures. **(D)** Control of seizure progression by MC modulation for seizures occurring during the daytime. Data analysis and presentation is similar as in Figure 3, but restricted to seizures occurring during the daytime. Top: Light treatment during daytime electrographic seizures on seizure progression has opposite effects in ChR2- and ArchT-expressing animals, and no effect on GFP control animals. Data are shown as the observed fraction of daytime convulsive seizures occurring after light delivery (color bars) compared with the fraction one would observe under the null hypothesis that light delivery has no effect (gray bars: expected fraction and 95% confidence interval, Monte-Carlo simulation). Bottom: for each measured animal (n = 4), photoinhibition of MCs significantly increases the occurrence of daytime convulsive seizures. Middle: photostimulation of MCs reduces the frequency of convulsive seizures (n = 5 animals). Right: light delivery to opsin-negative control mice does not affect convulsive seizure occurrence (n = 3 animals). $*P < 0.05$, $**P < 0.01$, two-tailed binomial test. **(E)** Same as in **(D)** for convulsive seizures occurring during nighttime. $ mouse not monitored continuously.

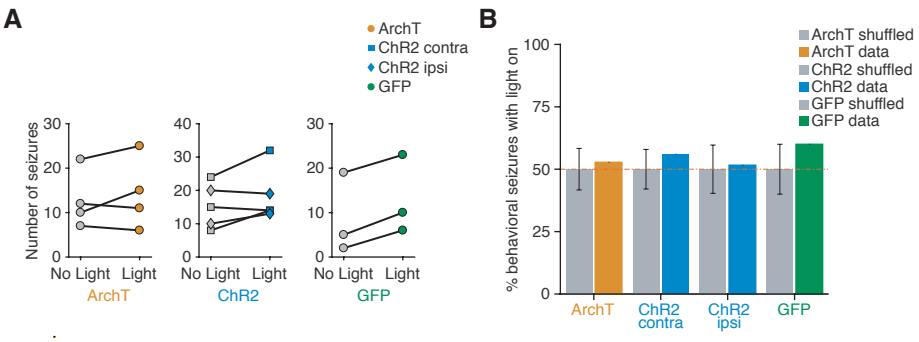

Figure S14. Test of causality: light delivery following the end of the convulsive seizure does not correlate with seizure occurrence. (A) Number of convulsive seizures followed by either a light or no light trigger (post-seizure trigger). Light and no light post-seizure triggers are equally likely to occur in all ArchT- (left; n = 4 mice), ChR2- (middle; n = 5 mice) or GFP- (right; n = 3 mice) expressing mice. This is in contrast with the data shown in Fig. 3 for pre-convulsive seizure triggers, which demonstrates that the relationship between pre-convulsive seizure trigger type (light vs. no light) and convulsive seizure occurrence is causal and not due to selection bias or artifacts in light delivery. **(B)** The measured fraction of convulsive seizures followed by a light trigger (colored bars) falls in the range expected under the null hypothesis that post-seizure light delivery has no effect on the occurrence of convulsive seizure (gray bars show the mean fraction and 95% CI for a binomial distribution with 50% success rate). Contra, contralateral to the kainate injection site; ipsi, ipsilateral to the kainate injection site.

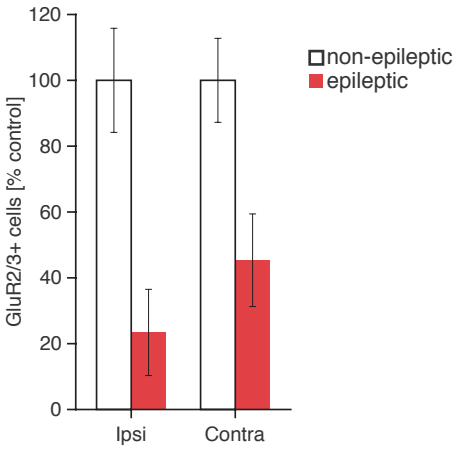

Figure S15. Hilar mossy cell loss in mice with chronic TLE. Number of GluR2/3+ cells in epileptic animals (N = 33 slices, n = 3 mice), compared with and normalized to non-epileptic controls (N = 35 slices, n = 3 mice). All data are presented as mean ± s.e.m. Ipsi, ipsilateral to the site of KA injection; contra, contralateral to the site of KA injection.

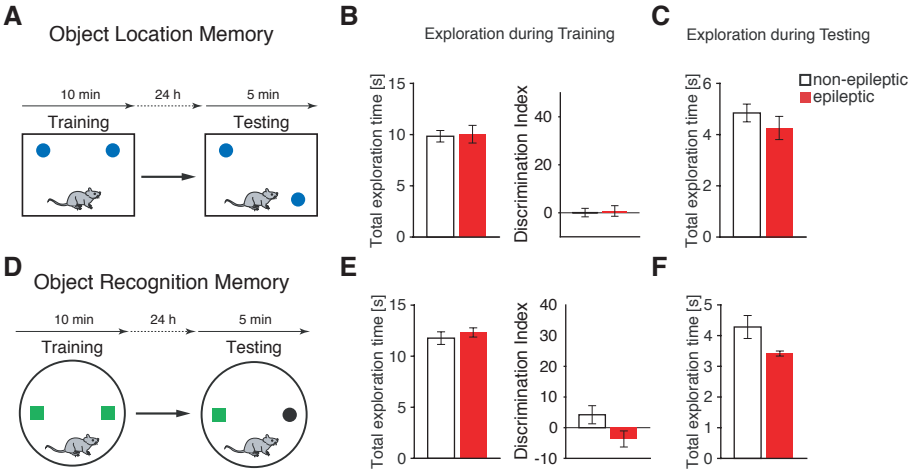

Figure S16. Object exploration during Object Location Memory and Object Recognition Memory in epileptic mice. **(A-C)** Epileptic mice do not have significantly different total exploration times as compared with their non-epileptic littermates during the **(B, left)** training or **(C)** testing phases of the OLM task, and **(B, right)** mice do not exhibit a side preference during OLM training (n = 13 non-epileptic mice, n = 17 epileptic mice; $P > 0.05$, two-tailed Welch's t-test). **(D-F)** Epileptic mice do not have significantly different total exploration times as compared with their non-epileptic littermates during the **(E, left)** training or **(F)** testing phases of the ORM task, and **(E, right)** mice do not exhibit a side preference during ORM training (n = 10 non-epileptic mice, n = 14 epileptic mice; $P > 0.05$, two-tailed Welch's t-test).

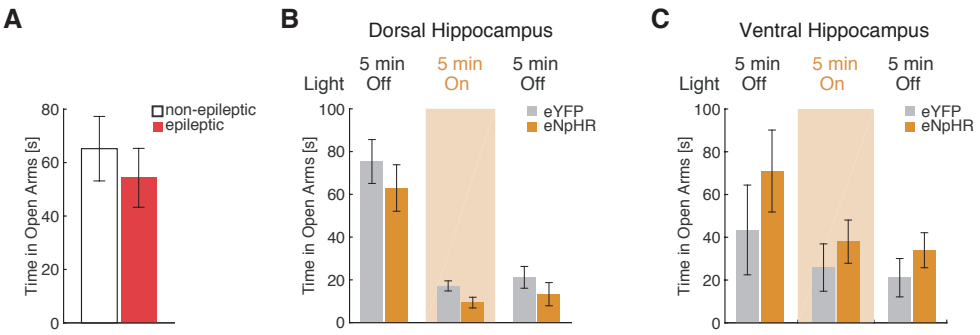

Figure S17. Epileptic mice do not have altered levels of anxiety, and anxiety is not altered with mossy cell inhibition. **(A)** Non-epileptic (n = 12) and epileptic (n = 10) mice do not have significantly different levels of anxiety as assessed by the time spent in the open arms of the elevated plus maze. **(B)** MC photoinhibition in the dorsal hippocampus does not alter time spent in the open arms of the EPM (n = 9 eYFP, n = 8 eNpHR). **(C)** MC photoinhibition in the ventral hippocampus does not alter time spent in the open arms of the EPM (n = 10 eYFP, n = 12 eNpHR). Shaded orange boxes indicate epochs of light delivery. All data are presented as mean ± s.e.m. $P > 0.05$, two-tailed Welch's t-test.

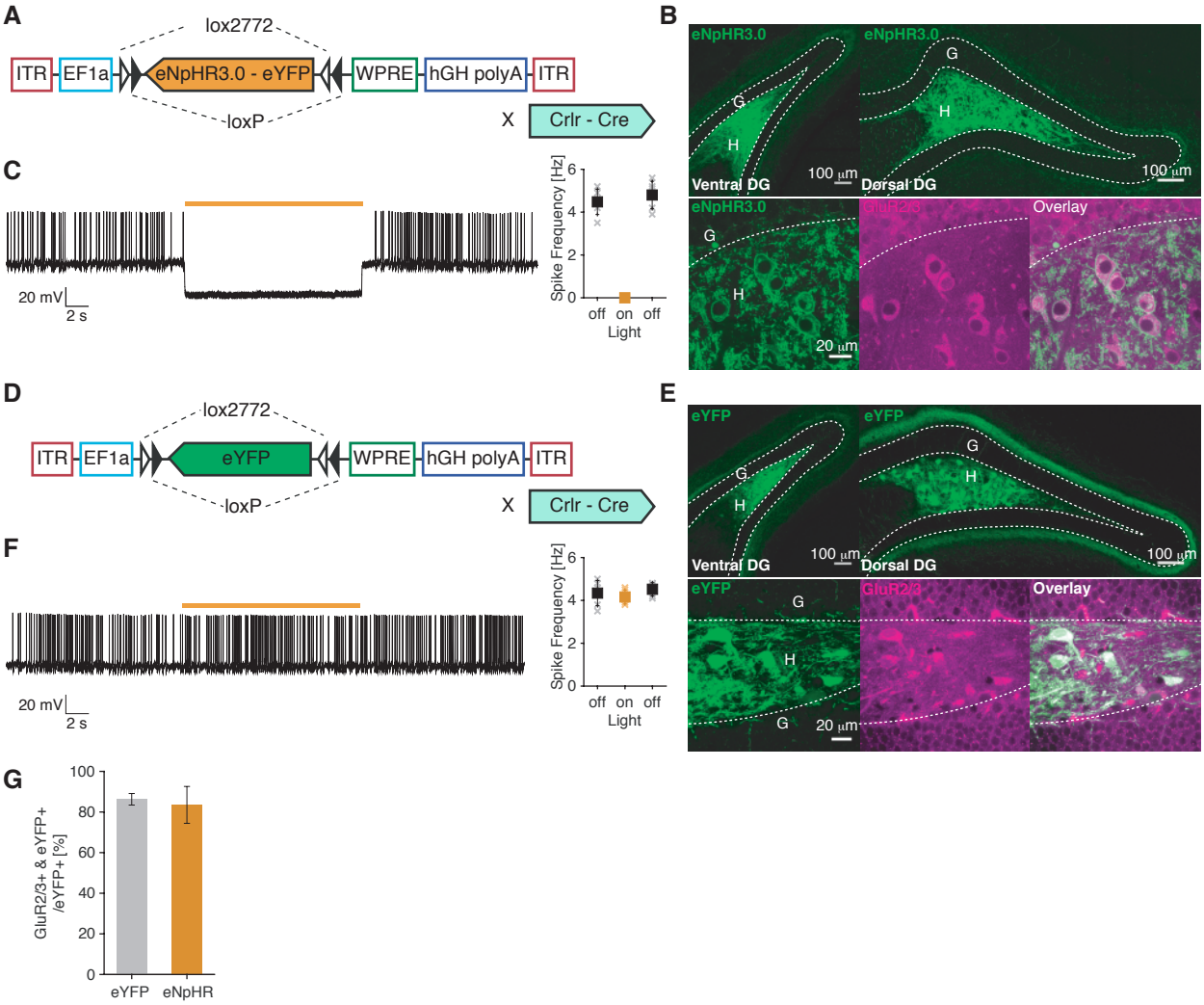

Figure S18. Selective optogenetic control of hippocampal dentate gyrus mossy cells. (A) Cre-dependent eNpHR expression system. **(B)** Top: confocal images of eNpHR expression in the ventral (left) and dorsal (right) DG. Bottom: high magnification images of the DG showing eNpHR-expressing MCs identified via eYFP expression and GluR2/3+ immunostaining. **(C)** 15 second illumination blocks current-induced spiking in eNpHR-expressing MCs, quantified on the right (N = 5 recordings, n = 3 mice). **(D)** Cre-dependent eYFP expression system. **(E)** Top: confocal images of eYFP expression in the ventral (left) and dorsal (right) DG. Bottom: high magnification images of the DG showing eYFP-expressing MCs identified via eYFP expression and GluR2/3+ immunostaining. **(F)** 15 second illumination has no effect on eYFP-expressing MCs in opsin-negative control mice, quantified on the right (N = 5 recordings, n = 3 mice). **(G)** Opsin expression specificity, quantified by the proportion of eNpHR+ neurons that were also GluR2/3+ (N = 33 slices, n = 3 mice) and of eYFP+ neurons that were also GluR2/3+ (N = 16 slices, n = 3 mice) showed similar, high levels of opsin expression specificity. All data are presented as mean ± s.e.m. G, granule cell layer; H, hilus.

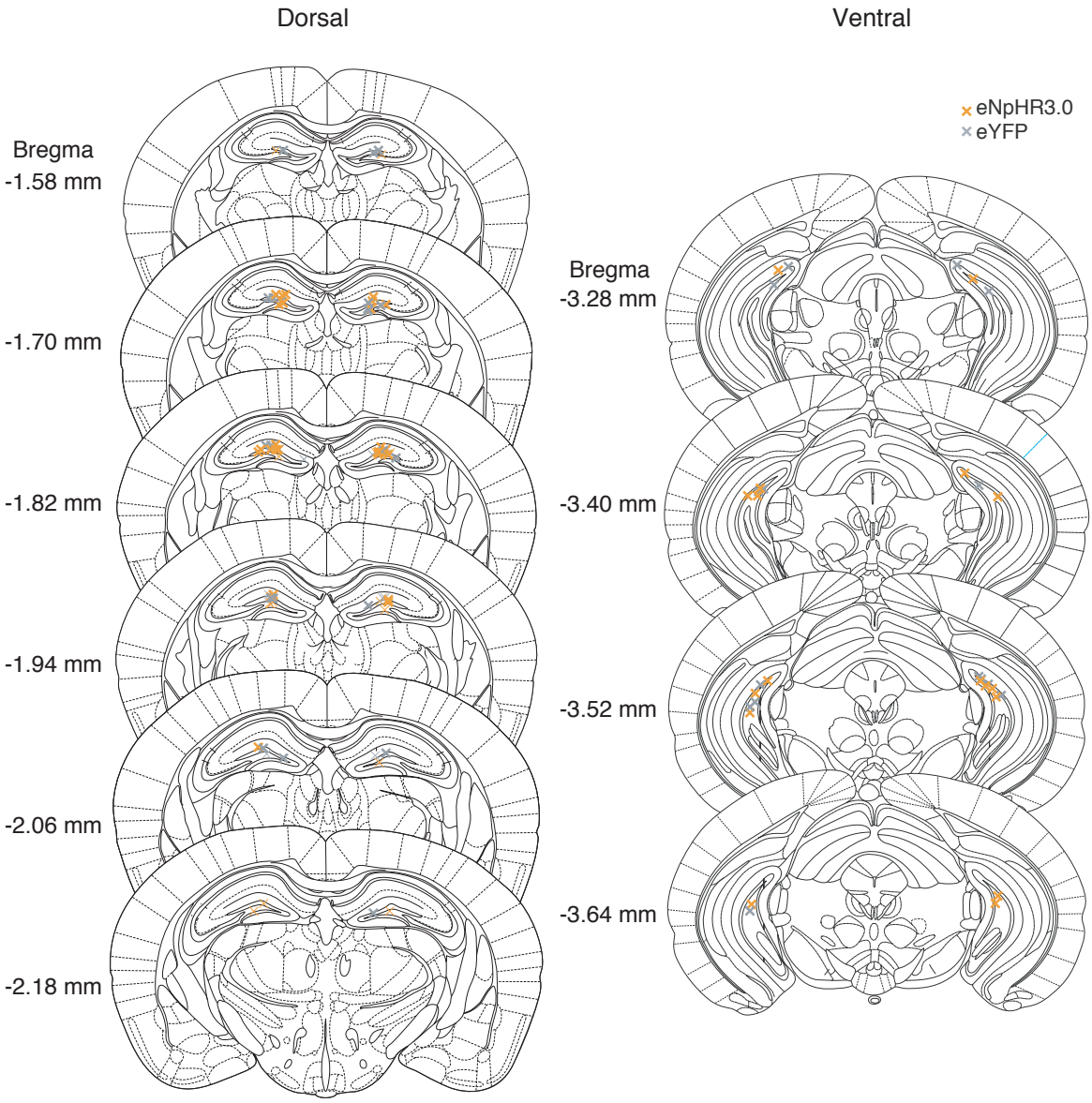

Figure S19. Post-hoc verification of optical fiber locations for OLM, ORM, and EPM mice. (n = 18 eNpHR dorsal, n = 18 eYFP dorsal, n = 10 eNpHR ventral, n = 8 eYFP ventral).

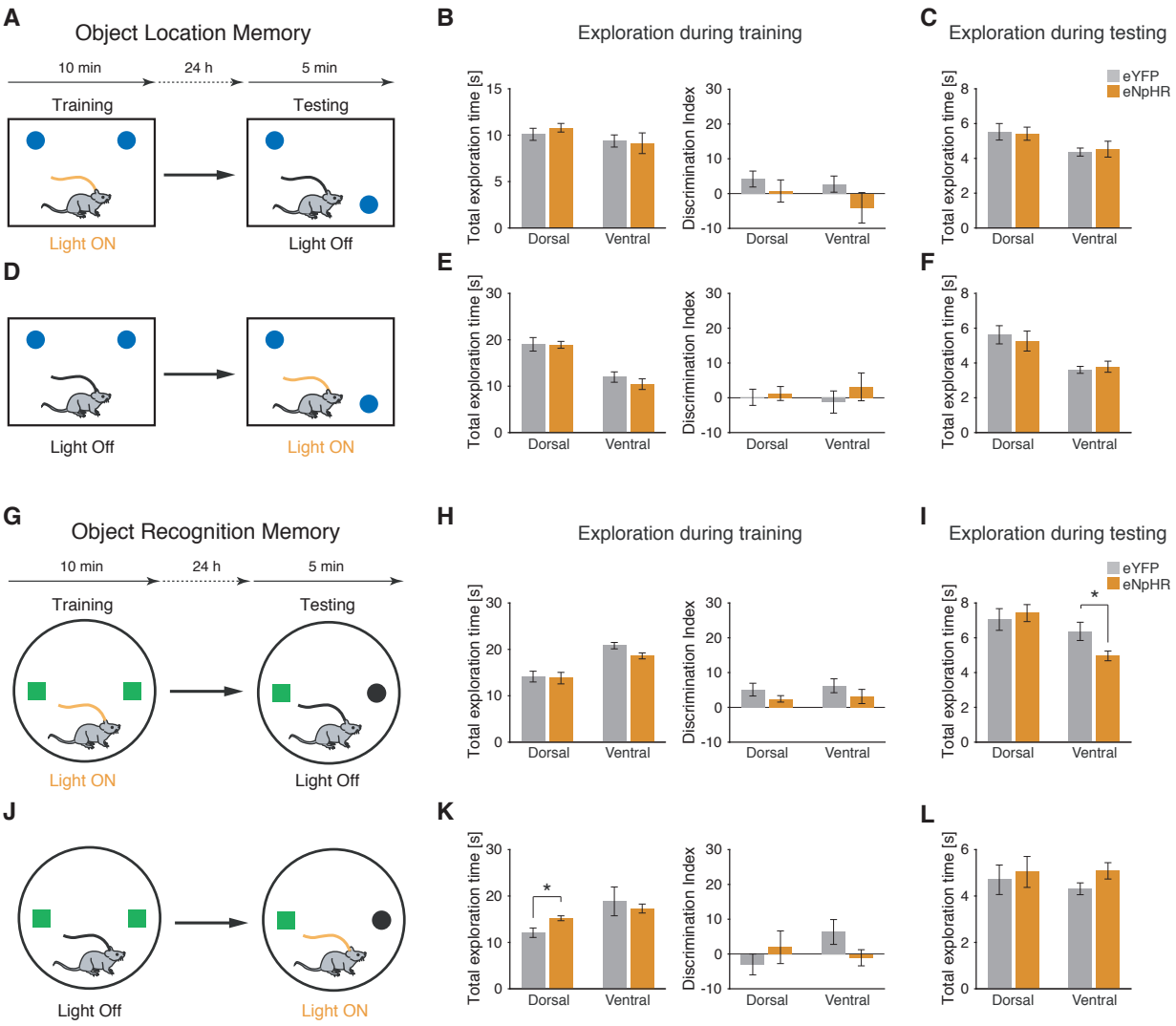

Figure S20. Object exploration during Object Location Memory and Object Recognition Memory. **(A-C)** MC photoinhibition during training of the OLM task does not alter total exploration time of objects during the **(B, left)** training or **(C)** testing phases, and **(B, right)** mice do not exhibit a side preference during training (dorsal: n = 9 eYFP, n = 10 eNpHR; ventral: n = 8 eYFP, n = 5 eNpHR). **(D-F)** MC photoinhibition specifically during testing of OLM does not alter total exploration time of objections during the **(E, left)** training or **(F)** testing phases, and **(E, right)** mice do not exhibit a side preference during training. (dorsal: n = 9 eYFP, n = 8 eNpHR; ventral: n = 6 eYFP, n = 7 eNpHR). **(G-I)** MC photoinhibition during training of the ORM task does not alter total exploration time of objects during the **(H, left)** training or **(I)** testing phases, and **(H, right)** mice do not exhibit a side preference during training (dorsal: n = 10 eYFP, n = 10 eNpHR; ventral: n = 9 eYFP, n = 10 eNpHR). **(J-L)** MC photoinhibition specifically during testing of ORM does not alter total exploration time of objects during the **(K, left)** training or **(L)** testing phases, and **(K, right)** mice do not exhibit a side preference during training (dorsal: n = 10 eYFP, n = 10 eNpHR; ventral: n = 7 eYFP, n = 9 eNpHR). *$P < 0.05$, two-tailed Welch's t-test.

Table S1. Intrinsic physiological properties of MCs from opsin- and GFP-expressing MCs in non-epileptic and epileptic mice. N = 5|5|10|5 cells from non-epileptic with opsin|non-epileptic without opsin|epileptic with opsin|epileptic without opsin mice. Values are expressed as mean ± s.e.m.

Table S2. Properties and effect of light delivery on individual juxtacellularly-recorded dentate gyrus neurons in non-epileptic and epileptic, ChR2-expressing and opsin-negative mice.

Table S3. Statistics of optogenetic MC modulation on electrographic seizure duration after and before light or sham trigger. We examined the mean and median seizure duration after or before the trigger, relative light/sham seizure duration, and compared the durations using a non-parametric Mann-Whitney *U* test.

Table S4. Raw data for object exploration during OLM and ORM training and testing for non-epileptic vs. epileptic mice as well as for eYFP- vs. eNpHR-expressing mice. t_L object, time spent exploring left object (s); t_R object, time spent exploring right object (s); t_total, total time spent exploring both objects; DI, discrimination index (see Experimental procedures); Tr, training; Te, testing; L, light; D, dorsal hippocampus; V, ventral hippocampus. Under Test, test performed is represented as: "task and phase_L light on for phase_light delivery location". For example, "OLMTr_LTe_D" represents data for the OLM task during the training phase, light is on during the testing phase, light is delivered to the dorsal hippocampus.

References

1. P. Kwan, J. W. Sander, The natural history of epilepsy: An epidemiological view. *J. Neurol. Neurosurg. Psychiatry* **75**, 1376–1381 (2004). doi:10.1136/jnnp.2004.045690 Medline

2. I. Blümcke, B. Suter, K. Behle, R. Kuhn, J. Schramm, C. E. Elger, O. D. Wiestler, Loss of hilar mossy cells in Ammon's horn sclerosis. *Epilepsia* **41** (Suppl 6), S174–S180 (2000). doi:10.1111/j.1528-1157.2000.tb01577.x Medline

3. H. E. Scharfman, The enigmatic mossy cell of the dentate gyrus. *Nat. Rev. Neurosci.* **17**, 562–575 (2016). doi:10.1038/nrn.2016.87 Medline

4. Ad. Ratzliff, A. L. Howard, V. Santhakumar, I. Osapay, I. Soltesz, Rapid deletion of mossy cells does not result in a hyperexcitable dentate gyrus: Implications for epileptogenesis. *J. Neurosci.* **24**, 2259–2269 (2004). doi:10.1523/JNEUROSCI.5191-03.2004 Medline

5. R. S. Sloviter, C. A. Zappone, B. D. Harvey, A. V. Bumanglag, R. A. Bender, M. Frotscher, "Dormant basket cell" hypothesis revisited: Relative vulnerabilities of dentate gyrus mossy cells and inhibitory interneurons after hippocampal status epilepticus in the rat. *J. Comp. Neurol.* **459**, 44–76 (2003). doi:10.1002/cne.10630 Medline

6. V. Gradinaru, F. Zhang, C. Ramakrishnan, J. Mattis, R. Prakash, I. Diester, I. Goshen, K. R. Thompson, K. Deisseroth, Molecular and cellular approaches for diversifying and extending optogenetics. *Cell* **141**, 154–165 (2010). doi:10.1016/j.cell.2010.02.037 Medline

7. S. Jinde, V. Zsiros, Z. Jiang, K. Nakao, J. Pickel, K. Kohno, J. E. Belforte, K. Nakazawa, Hilar mossy cell degeneration causes transient dentate granule cell hyperexcitability and impaired pattern separation. *Neuron* **76**, 1189–1200 (2012). doi:10.1016/j.neuron.2012.10.036 Medline

8. A. Bragin, J. Engel Jr., C. L. Wilson, E. Vizentin, G. W. Mathern, Electrophysiologic analysis of a chronic seizure model after unilateral hippocampal KA injection. *Epilepsia* **40**, 1210–1221 (1999). doi:10.1111/j.1528-1157.1999.tb00849.x Medline

9. F. Volz, H. H. Bock, M. Gierthmuehlen, J. Zentner, C. A. Haas, T. M. Freiman, Stereologic estimation of hippocampal GluR2/3- and calretinin-immunoreactive hilar neurons (presumptive mossy cells) in two mouse models of temporal lobe epilepsy. *Epilepsia* **52**, 1579–1589 (2011). doi:10.1111/j.1528-1167.2011.03086.x Medline

10. E. Krook-Magnuson, C. Armstrong, M. Oijala, I. Soltesz, On-demand optogenetic control of spontaneous seizures in temporal lobe epilepsy. *Nat. Commun.* **4**, 1376 (2013). doi:10.1038/ncomms2376 Medline

11. E. Krook-Magnuson, C. Armstrong, A. Bui, S. Lew, M. Oijala, I. Soltesz, In vivo evaluation of the dentate gate theory in epilepsy. *J. Physiol.* **593**, 2379–2388 (2015). doi:10.1113/JP270056 Medline

12. P. S. Buckmaster, H. J. Wenzel, D. D. Kunkel, P. A. Schwartzkroin, Axon arbors and synaptic connections of hippocampal mossy cells in the rat in vivo. *J. Comp. Neurol.* **366**, 270–292 (1996). doi:10.1002/(SICI)1096-9861(19960304)366:2<270:AID-CNE7>3.0.CO;2-2 Medline

13. R. J. Racine, Modification of seizure activity by electrical stimulation. II. Motor seizure. *Electroencephalogr. Clin. Neurophysiol.* **32**, 281–294 (1972). doi:10.1016/0013-4694(72)90177-0 Medline

14. J. Dyhrfjeld-Johnsen, V. Santhakumar, R. J. Morgan, R. Huerta, L. Tsimring, I. Soltesz, Topological determinants of epileptogenesis in large-scale structural and functional models of the dentate gyrus derived from experimental data. *J. Neurophysiol.* **97**, 1566–1587 (2007). doi:10.1152/jn.00950.2006 Medline

15. A. Vogel-Ciernia, D. P. Matheos, R. M. Barrett, E. A. Kramár, S. Azzawi, Y. Chen, C. N. Magnan, M. Zeller, A. Sylvain, J. Haettig, Y. Jia, A. Tran, R. Dang, R. J. Post, M. Chabrier, A. H. Babayan, J. I. Wu, G. R. Crabtree, P. Baldi, T. Z. Baram, G. Lynch, M. A. Wood, The neuron-specific chromatin regulatory subunit BAF53b is necessary for synaptic plasticity and memory. *Nat. Neurosci.* **16**, 552–561 (2013). doi:10.1038/nn.3359 Medline

16. H. Lin, G. L. Holmes, J. L. Kubie, R. U. Muller, Recurrent seizures induce a reversible impairment in a spatial hidden goal task. *Hippocampus* **19**, 817–827 (2009). doi:10.1002/hipo.20565 Medline

17. C. R. Houser, Granule cell dispersion in the dentate gyrus of humans with temporal lobe epilepsy. *Brain Res.* **535**, 195–204 (1990). doi:10.1016/0006-8993(90)91601-C Medline

18. M. Mahn, M. Prigge, S. Ron, R. Levy, O. Yizhar, Biophysical constraints of optogenetic inhibition at presynaptic terminals. *Nat. Neurosci.* **19**, 554–556 (2016). doi:10.1038/nn.4266 Medline

19. G. Buzsáki, E. Eidelberg, Commissural projection to the dentate gyrus of the rat: Evidence for feed-forward inhibition. *Brain Res.* **230**, 346–350 (1981). doi:10.1016/0006-8993(81)90413-3 Medline

20. T.-T. Hsu, C.-T. Lee, M.-H. Tai, C.-C. Lien, Differential recruitment of dentate gyrus interneuron types by commissural versus perforant pathways. *Cereb. Cortex* **26**, 2715–2727 (2016). doi:10.1093/cercor/bhv127 Medline

21. Y. Sugaya, M. Yamazaki, M. Uchigashima, K. Kobayashi, M. Watanabe, K. Sakimura, M. Kano, Crucial roles of the endocannabinoid 2-arachidonoylglycerol in the suppression of epileptic seizures. *Cell Reports* **16**, 1405–1415 (2016). doi:10.1016/j.celrep.2016.06.083 Medline

22. Y. Senzai, G. Buzsáki, Physiological properties and behavioral correlates of hippocampal granule cells and mossy cells. *Neuron* **93**, 691–704.e5 (2017). doi:10.1016/j.neuron.2016.12.011 Medline

23. D. GoodSmith, X. Chen, C. Wang, S. H. Kim, H. Song, A. Burgalossi, K. M. Christian, J. J. Knierim, Spatial representations of granule cells and mossy cells of the dentate gyrus. *Neuron* **93**, 677–690.e5 (2017). doi:10.1016/j.neuron.2016.12.026 Medline

24. N. B. Danielson, G. F. Turi, M. Ladow, S. Chavlis, P. C. Petrantonakis, P. Poirazi, A. Losonczy, In vivo imaging of dentate gyrus mossy cells in behaving mice. *Neuron* **93**, 552–559.e4 (2017). doi:10.1016/j.neuron.2016.12.019 Medline

25. M. A. Kheirbek, L. J. Drew, N. S. Burghardt, D. O. Costantini, L. Tannenholz, S. E. Ahmari, H. Zeng, A. A. Fenton, R. Hen, Differential control of learning and anxiety along the

dorsoventral axis of the dentate gyrus. *Neuron* **77**, 955–968 (2013). doi:10.1016/j.neuron.2012.12.038 Medline

26. J.-M. Zhuo, H. A. Tseng, M. Desai, M. E. Bucklin, A. I. Mohammed, N. T. M. Robinson, E. S. Boyden, L. M. Rangel, A. P. Jasanoff, H. J. Gritton, X. Han, Young adult born neurons enhance hippocampal dependent performance via influences on bilateral networks. *eLife* **5**, e22429 (2016). doi:10.7554/eLife.22429 Medline

27. R. A. Hyde, B. W. Strowbridge, Mnemonic representations of transient stimuli and temporal sequences in the rodent hippocampus in vitro. *Nat. Neurosci.* **15**, 1430–1438 (2012). doi:10.1038/nn.3208 Medline

28. C. Armstrong, E. Krook-Magnuson, M. Oijala, I. Soltesz, Closed-loop optogenetic intervention in mice. *Nat. Protoc.* **8**, 1475–1493 (2013). doi:10.1038/nprot.2013.080 Medline

29. S. Klein, M. Bankstahl, W. Löscher, Inter-individual variation in the effect of antiepileptic drugs in the intrahippocampal kainate model of mesial temporal lobe epilepsy in mice. *Neuropharmacology* **90**, 53–62 (2015). doi:10.1016/j.neuropharm.2014.11.008 Medline

30. G. G. Szabo, X. Du, M. Oijala, C. Varga, J. M. Parent, I. Soltesz, Extended interneuronal network of the dentate gyrus. *Cell Reports* **20**, 1262–1268 (2017). doi:10.1016/j.celrep.2017.07.042 Medline

31. A. Vogel-Ciernia, M. A. Wood, in *Current Protocols in Neuroscience* (Wiley, Hoboken, NJ, USA, 2014), p. 8.31.1–8.31.17.